

# ATCA observations of SiO masers in the Galactic center

Juan Li<sup>1,2,3</sup>, Tao An<sup>1</sup>, Zhi-Qiang Shen<sup>1,2</sup>, Atsushi Miyazaki<sup>4</sup>

## ABSTRACT

We present the Australia Telescope Compact Array (ATCA) observations of the SiO masers in the Galactic center in transitions of  $v=1, J=2-1$  at 86 GHz and  $v=1, J=1-0$  at 43 GHz. Two 86-GHz SiO masers were detected within the central parsec, and they are associated with IRS 10EE and IRS 15NE, respectively. We detected eighteen 43-GHz SiO masers within a projected separation of  $\lesssim 2$  pc from Sagittarius A\* (Sgr A\*), among which seven masers are newly discovered from our observations. This raises the total number of 43-GHz SiO masers within the central 4 parsecs of the GC region to 22. Simultaneous observations at 86 and 43 GHz showed that the intensity of 43-GHz SiO maser is  $\sim 3$  times higher than that of 86-GHz maser in IRS 10EE (an OH/IR star), while the integrated flux of the SiO maser emission at 43 GHz is comparable with that at 86 GHz in IRS 15NE (an ordinary Mira variable). These results are consistent with previous observations of massive late-type stars in the Galaxy in which the 86-GHz SiO maser is in general weaker than the 43-GHz SiO maser in OH/IR stars, while the two transitions are comparably strong in Mira stars.

*Subject headings:* Galaxy: center— masers— radio lines: stars— circumstellar matter— stars: late-type

## 1. Introduction

---

<sup>1</sup>Shanghai Astronomical Observatory, Chinese Academy of Sciences, Shanghai 200030, China; lijuan@shao.ac.cn; antao@shao.ac.cn, zshen@shao.ac.cn

<sup>2</sup>Joint Institute for Galaxy and Cosmology (JOINGC) of SHAO and USTC, Shanghai 200030, China;

<sup>3</sup>Department of Astronomy, Nanjing University, Nanjing 210093, China;

<sup>4</sup>Mizusawa VLBI Observatory, National Astronomical Observatory of Japan, Mizusawa, Oshu, Iwate 023-0861, Japan; amiya@miz.nao.ac.jp

SiO masers located in the extended circumstellar envelopes of late-type giant stars are believed to be reliable tracers of the Galactic dynamics since they can be treated as point-like objects and are not subject to non-gravitational forces such as magnetic fields or stellar wind collisions. A number of SiO maser surveys toward the Galactic center (GC) region have been carried out at 43 GHz in order to study the structure and dynamics of the stellar disk in the Inner Galaxy (Izumiura et al. 1998; Miyazaki et al. 2001; Deguchi et al. 2000, 2002; Sjouwerman et al. 2002, 2004; Imai et al. 2002). So far the most sensitive search for 43-GHz SiO masers in the central few parsec region of the GC was made with the VLA and VLBA, and the accurate position determination of the SiO masers has been used to calibrate the astrometry in the infrared images of the same region with an accuracy of  $\sim 1$  mas (Menten et al. 1997; Reid et al. 2003, 2007; Oyama et al. 2008). Moreover fifteen SiO maser sources have been observed with a projected separation  $< 50''$  from Sgr A\* at 43 GHz; lower limit of the dynamic mass enclosed within a given radius was derived from the 3-dimensional velocity of the maser star. Whereas only in IRS 9, the derived enclosed mass limit is  $\sim 20$  percent higher than the mass of known objects in the GC, i.e., the supermassive black hole (SMBH) and the luminous stars (Reid et al. 2007). In fact previous VLA observations of SiO masers were constrained by the limited velocity coverage of the receiver band. Searching for high-velocity SiO maser stars is critical for exploring the mass distribution in the GC.

At 86 GHz, Lindqvist et al. (1991) searched for SiO maser line emission in a sample of 31 OH/IR stars close to the GC using the Nobeyama 45m telescope, but they failed to obtain distinctive detection of any 86 GHz masers. Messineo et al. (2002) detected 271 SiO masers in a sample of 441 late-type stars in the Inner Galaxy from their high-sensitivity IRAM-30m observations. Limited by the low angular resolution and sensitivity of single-dish observations, the number and spatial distribution of SiO maser sources within a few parsecs of the GC remain uncertain. Until recently, high-angular-resolution observations of 86-GHz SiO maser line emission from the GC have been made possible using the Australia Telescope Compact Array (ATCA) of the Australia Telescope National Facility (ATNF) (this paper and L.O. Sjouwerman et al., private communication).

In addition to the important role on accurate astrometry, SiO maser is also an excellent probe of the physical condition in the circumstellar envelope. VLBI observations of SiO masers in massive late-type stars distributed in the Galactic disk showed that these maser spots are located in the innermost ( $\sim 4$ – $8$  AU) regions of the circumstellar envelopes of the stars (Diamond & Kemball 2003), whereas the pumping mechanism of the SiO maser line is still an open question (Doel et al. 1995; Desmurs et al. 2000; Humphreys et al. 2002). The SiO masers are strongly variable over timescales of  $\sim 1$  yr, therefore simultaneous observations of the GC SiO masers at multiple transitions would provide helpful information for constraining the excitation conditions of the SiO maser lines under extreme astrophysical

environment.

In this Letter, we present the results from the ATCA observations of SiO maser lines at two transitions ( $v=1, J=2-1$  (86 GHz) and  $v=1, J=1-0$  (43 GHz)) within a few parsecs from Sgr A\*. The ATCA observations and data reduction are described in Section 2, and the results and analysis are presented in Section 3. In Section 4 we summarize the observational results. Throughout this paper we adopt a GC distance of 8 kpc (Reid 1993) and a SMBH mass of  $4 \times 10^6 M_{\odot}$  at the GC (Ghez et al. 2008; Gillessen et al. 2009).

## 2. OBSERVATIONS AND DATA REDUCTION

We carried out ATCA observations of the Galactic center at 86 and 43 GHz in five sessions (2006 June 9, 2006 August 13, 2007 October 21, 2008 June 3-4 and 2008 October 3). These observations were initially made with the purpose of investigating the variability of Sgr A\* at millimeter wavelengths (Li et al. 2009). The observations on 2008 October 3 were made quasi simultaneously at 43 and 86 GHz by interchanging the receivers at the two frequencies with a duty cycle of about 20 minutes. The observations on other dates were performed solely at a single frequency. Except for the observation on 2008 June 3-4, other observations were made under good weather condition. Table 1 summarizes the observational parameters.

Quasar 3C 279 was observed at the beginning of each observing run to calibrate the bandpass. The observations were pointed at Sgr A\*, allowing for detection of SiO masers located in the primary beam of the ATCA antenna, i.e.,  $\theta_{FWHP}$  of  $\sim 36''$  and  $\sim 72''$  at 86 and 43 GHz, respectively. The pointing were checked and corrected every half an hour by observing either a nearby quasar PKS 1730-130 (NRAO 530) or a strong SiO maser VX Sgr. Quasar PKS 1741-312 and SiO maser OH 2.6–0.4 were interlaced with Sgr A\* to track the elevation-dependent gains.

The data were reduced using the *MIRIAD* package<sup>1</sup>. We first calibrated the bandpass and elevation-dependent complex gains following the standard procedure described in the *MIRIAD* Cookbook. Next we derived the flux density scale for the visibility data observed in 2007 and 2008 using the planet Uranus. The resulting uncertainty of the absolute flux density was  $\lesssim 20\%$ . For the observations in 2006, the Uranus was resolved, therefore the flux density scale was determined from the quasar NRAO 530 on 2006 June 9 (2.27 Jy from the ATCA calibrator monitoring program) and from PKS 1921-293 (8.44 Jy) on 2006 August

---

<sup>1</sup><http://www.atnf.csiro.au/computing/software/miriad/>

13, respectively. Then we made a continuum map of the Galactic center from the visibilities on line-free channels and further carried out a few iterations of phase-only self-calibration to correct residual phase errors. The gain solutions derived from the continuum data were transferred and applied to the line data. Using *MIRIAD* task UVLIN, the continuum level was determined by a linear fitting to the line-free channels and was subtracted from the calibrated line data in the  $uv$  plane. A spectral-line cube was constructed from mapping the continuum-subtracted data. In order to increase the sensitivity in the channel maps, we have smoothed the line data to a velocity resolution of  $1 \text{ km s}^{-1}$  at 86 GHz and  $2 \text{ km s}^{-1}$  at 43 GHz. The typical *rms* noise in individual channels is 5 mJy at 43 GHz, and 13–55 mJy at 86 GHz, depending on the weather condition and effective integration time (see Table 1).

We searched for SiO maser sources within a radius of  $25''$  and  $50''$  centering at Sgr A\* at 86 and 43 GHz, respectively. For those SiO maser sources detected above  $5\sigma$ , we derived their positions in two steps: first, we fitted their brightness distribution with a two-dimensional Gaussian using the task IMFIT in each channel; then, we made variance-weighted averaging to obtain its mean position and the uncertainty.

### 3. RESULTS AND ANALYSIS

#### 3.1. 86 GHz masers

Two SiO masers were detected in the 86 GHz images with peak flux densities higher than  $5\sigma$ . These two sources were identified to be associated with IRS 10EE and IRS 15NE, based on the consistent positions and radial velocities determined from previous observations (Reid et al. 2003, 2007). IRS 10EE appeared at four epochs ( $\sim 4\sigma$  on 2008 October 3) and displayed strong variability on timescale of months. IRS 15NE was only distinctively detected on 2007 October 21. It was marginally detected on 2008 June 4 ( $\sim 3\sigma$ ) as a result of high *rms* noise level. The late-type giants and supergiants in the GC are likely detectable over a wide radial velocity range of  $\pm 350 \text{ km s}^{-1}$  (e.g., Figer et al. 2003). However, current 86-GHz observations were constrained by the limited velocity coverage and relatively low sensitivity. The positions, peak flux densities and velocity-integrated flux densities of IRS 10EE and IRS 15NE are listed in Table 2. The *rms* noise of the integrated flux density is estimated as  $\Delta I = \sigma_{rms} \Delta v (N_{chan})^{1/2}$ , where  $\sigma_{rms}$  is the *rms* noise level in individual channel maps,  $\Delta v$  is the velocity resolution, and  $N_{chan}$  is the number of channels over which the  $\Delta I$  is calculated (Klaassen & Wilson 2007).

We will comment on these two 86-GHz maser sources as follows.

- (1) *IRS 10EE* was identified as an OH/IR star and has been observed with SiO, OH and

H<sub>2</sub>O maser line emission (Lindqvist et al. 1990, 1992; Menten et al. 1997; Sjouwerman et al. 2002; Reid et al. 2003, 2007; Oyama et al. 2008; Peeples et al. 2007). In infrared (IR) bands it was classified as a long-period variable, and exhibited variability on various timescales ranging from several days to a few months (Tamura et al. 1996; Wood et al. 1998; Ott et al. 1999; Peeples et al. 2007). X-ray emission was detected within 0."8 of IRS 10EE (Muno et al. 2004) and a binary system was proposed to explain its relatively high X-ray luminosity as an AGB star (Peeples et al. 2007). The binary scenario of IRS 10EE was further supported by the VLBA monitoring of its proper motion (Oyama et al. 2008). Spectra of 86- and 43-GHz SiO maser lines of IRS 10EE from our observations are shown in the upper panel of Figure 1. They indicated a flux density variation on timescale of months, in agreement with previous radio and IR observations. Long-term monitoring of SiO maser emission in IRS 10EE and comparison with the optical phase change would provide an important tool for understanding the pumping mechanisms in this source (Pardo et al. 2004).

(2) *IRS 15NE* showed not only strong characteristic cool star features, but broad He I and Br $\gamma$  emission in the IR spectrum, suggesting that it is a close blend (Genzel et al. 1996, 2000; Blum et al. 2003, Oyama et al. 2008). VLBA observations of IRS 15NE at 43 GHz showed that the maser source was only slightly resolved and extended with a diameter of about 2 mas (Oyama et al. 2008). This SiO maser source is relatively weak compared with IRS 10EE. It is variable at both 43 and 86 GHz (lower panel in Figure 1). The 43 GHz peak flux density on 2008 June 3 was only a seventh of that on 1998 observing epoch of Reid et al. (2003). The velocity of the peak 86-GHz maser feature changed from about  $-11.7$  km s<sup>-1</sup> on 2007 October 21 to about  $-13.0$  km s<sup>-1</sup> on 2008 June 4. For a star at a projected separation  $R$  from the GC, the radial-direction component of the acceleration,  $a_r$ , due to the gravitation of the enclosed mass  $M(r)$  can be calculated as:

$$\frac{a_r}{[km\ s^{-1}\ yr^{-1}]} = \frac{GM(r) \sin \alpha}{(\frac{R}{\cos \alpha})^2} \leq 0.05 \left(\frac{\theta}{10''}\right)^{-2} \left(\frac{M(r)}{4 \times 10^6 M_\odot}\right) \quad (1)$$

where  $G$  is the gravitational constant,  $\alpha$  is the angle between the radius vector to the star and the plane of the sky containing the central mass ( $0^\circ \leq \alpha \leq 90^\circ$ ), and  $\theta$  is the observed angular separation. The  $a_r$  gets its maximum value in the case of  $\alpha = 35^\circ$ . Calculations based on the observed parameters of IRS 15NE suggest that the acceleration caused by the enclosed mass is not significant and far lower than the rate of the peak velocity variation. On the other hand, IRS 15NE seems to be a special case showing large variation of the peak velocity at the 43 GHz (Table 2). Therefore, the observed variation of the peak velocity of IRS 15NE seems unlikely to be caused by the gravitation acceleration by the dynamic center of the GC. The resolution of current observations is not high enough to explore whether the changes of the peak velocity are related to the variation in the spatial distribution of the masering regions.

### 3.2. 43 GHz masers

Seventeen 43-GHz SiO masers were identified on 2008 June 3 based on both radial velocity and position information. Among them eleven sources have been observed previously (Menten et al. 1997; Reid et al. 2003, 2007) and six are newly detected. One of the six new SiO masers, offset ( $+0.''9$ ,  $-8.''0$ ) from Sgr A\*, was associated with IRS 14NE, a known AGB star (Blum et al. 1996; Ott et al. 1999; Peebles et al. 2007). Following the nomenclature of the GC SiO masers adopted by Reid et al. (2007), the other five new SiO masers were named as SiO-18 ( $-77.6$  km s $^{-1}$ ), SiO-19 ( $-29.4$  km s $^{-1}$ ), SiO-20 ( $-20.3$  km s $^{-1}$ ), SiO-21 ( $+13.8$  km s $^{-1}$ ) and SiO-22 ( $+33.6$  km s $^{-1}$ ) in a sequence of ascending velocity.

We detected fourteen 43-GHz SiO masers on 2008 October 3, among which eleven masers were in agreement with previous observations (Menten et al. 1997; Reid et al. 2003, 2007) and two masers (SiO-18 and SiO-22) were also found on 2008 June 3. The remaining one maser ( $V_{LSR} = +80$  km s $^{-1}$ ) was found at ( $+24.''0$ ,  $+20.''3$ ) northeast of Sgr A\* and represents a new detection. We named it as SiO-23.

These detections at both 86 and 43 GHz are tabulated in Table 2. Together with previous observations, our new detections of SiO masers in the GC raise the total number of the 43-GHz SiO masers in the central  $100''$  (or 4 pc) region to 22, increasing by  $\sim 50$  percent. Figure 2 shows composite spectra of the 43-GHz SiO masers derived from two observations in 2008. Figure 3 displays a sketch map of the 2-dimensional distribution of 43-GHz SiO masers in the inner  $100''$  region of the GC. The contours in Figure 3 represent the continuum emission at 43 GHz. It is interesting to note that almost all sources with negative radial velocities have projected separations away from Sgr A\* less than  $25''$  ( $\sim 1$  pc); while most sources with positive radial velocities are located at larger projected distances  $> 25''$ . The origin for such a velocity distribution of the GC SiO maser stars is not clear. The IR observations of the massive stars in the GC suggest that the red giants and supergiants are belonging to a relax system and show isotropic 3-dimensional velocity distribution. Was the systematic change of the radial velocities of the SiO maser stars related to an intrinsically extraordinary property of the SiO maser stars (different from those non-maser red giants) or just a selection effect? More observations using the ATCA and EVLA with receiver bandwidth that covers the full velocity range of the GC SiO masers are necessary to obtain a complete view of the radial velocity and spatial distribution of SiO masers in the GC region and thus to solve this velocity distribution puzzle.

### 3.3. Relative Strength of SiO Maser transitions

Figure 1 compares the SiO maser line spectra of IRS 10EE from the quasi-simultaneous observations at 86 and 43 GHz on 2008 June 4 and 2008 October 3, and the quasi-simultaneous spectra of IRS 15NE at 86 and 43 GHz on 2008 June 4. The 43-GHz integrated flux of IRS 10EE is about 3-5 times higher than that of 86 GHz in the two observations. Different from IRS 10EE, the 43 GHz integrated flux of IRS 15NE is comparable with that of 86 GHz. The different behaviors of the SiO maser line emission in IRS 10EE (an OH/IR star) and IRS 15NE (an ordinary Mira) seem to be consistent with previous observations of massive late-type stars in the Galaxy (Nyman et al. 1986, 1993; Lindqvist et al. 1992) which showed that the 86-GHz SiO maser emission was weak in OH/IR stars compared with ordinary Mira variables. The high mass loss rate in OH/IR stars results in much turbulence to quench the 86-GHz maser excitation, as provides a possible explanation for relatively weak 86-GHz SiO maser emission in OH/IR stars. The radiative pumping should yield similar 43- and 86-GHz SiO intensities over broad ranges of SiO densities and abundances, while the collisional pumping is sensitive to the SiO column density and may give rise to different spatial distribution and different intensities at 86 and 43 GHz (Phillips et al. 2003 and references therein). Although the low-resolution observations in the present paper are not allowed for inspecting the spatial correspondence of 43- and 86-GHz maser spots, the large discrepancy between the integrated flux of IRS 10EE at the two frequencies would suggest that the radiative pumping might not be the dominant mechanism in this source. On the other hand, the turbulent outflows in IRS 10EE make it difficult for the circumstellar envelope to sustain at a density of  $(4 - 6) \times 10^9 \text{ cm}^{-3}$ , which is a scope for the 86-GHz maser emission to be effectively amplified (Doel et al. 1995). For IRS 15NE, either radiative or collisional pumping may be responsible for the observed 43- and 86-GHz SiO maser emission. In order for the collisional mechanism to be at work for IRS 15NE, the  $\text{H}_2$  gas density in most regions of the envelope is required to be close to a critical density  $\sim 5 \times 10^9 \text{ cm}^{-3}$  (Doel et al. 1995). Long-term monitoring of the maser line and infrared emissions from the GC SiO maser stars might be helpful for understanding the connection between the SiO maser variability and the IR stellar pulsation cycle.

## 4. Conclusion

A well-distributed sample of SiO maser stars in both spatial and velocity spaces is crucial for revealing the enclosed mass as a function of the projected radius in the GC. We have made sensitive search for SiO masers in the central 4-pc region of the GC at 43 and 86 GHz using the ATCA. The observations resulted in a detection of two 86-GHz SiO masers and

eighteen 43-GHz masers, of which seven are discovered for the first time. Combined with previous observations (Reid et al. 2007), the total number of the 43-GHz SiO masers in GC region has been raised to 22. The current observations of the GC SiO masers mainly made with the ATCA and VLA are concentrated in the radial velocity range of  $\pm 100$  km  $s^{-1}$ . The updated broad-band observing facilities such as the ATCA (with the CABB) and the EVLA are excellent tools to gain a complete view of the distribution of GC SiO masers. In particular, monitoring the high-radial-velocity maser stars using the VLBI is especially important for constraining the mass distribution in the GC.

In addition, the relative strength of SiO masers between 43 and 86 GHz from the simultaneous observations of IRS 10EE tends to favor a collisional pumping mechanism in IRS 10EE. For IRS 15NE, either radiative or collisional pumping mechanism, or both, might be at work.

The Australia Telescope Compact Array is part of the Australia Telescope which is founded by the Commonwealth of Australia for operation as a National Facility managed by the CSIRO.

This work was supported in part by the National Natural Science Foundation of China (grants 10625314, 10633010 and 10821302), the CAS/SAFEA International Partnership Program for Creative Research Teams and the Knowledge Innovation Program of the Chinese Academy of Sciences (Grant No. KJCX2-YW-T03), and sponsored by the Program of Shanghai Subject Chief Scientist (06XD14024) and the National Key Basic Research Development Program of China (No. 2007CB815405, 2009CB24903). We thank Willem Baan for proof-reading and constructive comments on the manuscript. JL would like to thank helpful discussions with Lorant Sjouwerman on the ATCA observations, and Xi Chen, Yongjun Chen, Bing Jiang and Zhiyu Zhang for comments and suggestions on this work.

## REFERENCES

- Blum, R. D., Sellgren, K. & Depoy, D. L. 1996, *ApJ*, 112, 1988
- Deguchi, S., Fujii, T., Izumiura, H. et al. 2000, *ApJS*, 128, 571
- Deguchi, S., Fujii, T., Miyoshi, M. & Nakashima, J. 2002, *PASJ*, 54, 61
- Desmurs, J. F., Bujarrabal, V., Colomer, F. & Alcolea, J. 2000, *A&A*, 360, 189
- Diamond, P. J. & Kemball, A.J. 2003, *ApJ*, 599, 1372



- Doel, R. C., Gray, M. D., Humphreys, E. M. L., Braithwaite, M. R. & Field, D. 1995, *A&A*, 302, 797
- Figer, D. F., Gilmore, D., Kim, S. S., Morris, M., Backlin, E. E., McLean, I. S., Gibert, A. M., Graham, J. R., Larkin, J. E., Levenson, N. A., Teplitz, H. I., 2003, *ApJ*, 599, 1139
- Genzel, R., Thatte, N., Krabbe, A., Kroker, H., & Tacconi-Garman, L.E. 1996, *ApJ*, 472, 153
- Genzel, R., Pichon, C., Eckart, A. et al. 2000, *MNRAS*, 317, 348
- Ghez, A. M., Salim, S., Weinberg, N. N. et al. 2008, *ApJ*, 689, 1044
- Gillessen, S., Eisenhauer, F., Fritz, T. K. et al. 2009, *ApJ*, 707, L114
- Humphreys, E. M. L., Gray, M. D., Yates, J. A., Field, D., Bowen, G. H. & Diamond, P. J. 2002, *A&A*, 386, 256
- Imai, H., Deguchi, S. & Fujii, T. et al. 2002, *PASJ*, 54, L19
- Izumiura, H., Deguchi, S. & Fujii, T. 1998, *ApJ*, 494, L89
- Klaassen, P. D. & Wilson, C. D. 2007, *ApJ*, 663, 1092
- Li, J., Shen, Z. Q., Miyazaki, A. et al. 2009, *ApJ*, 700, 417
- Lindqvist, M., Winnberg, A. & Forster, J. R. 1990, *A&A*, 229, 165
- Lindqvist, M., Winnberg, A., Habing, H. J. & Matthews, H. E. 1992, *A&AS*, 92, 43
- Lindqvist, M., Winnberg, A. Johansson, L. E. B. & Ukita, N. 1991, *A&A*, 250, 431
- Menten, K. M., Reid, M. J., Eckart, A. & Genzel, R. 1997, *ApJ*, 475, L111
- Messineo, M., Habing, H. J., Sjouwerman, L. O. et al. 2002, *A&A*, 393, 115
- Miyazaki, A., Deguchi, S., Tsuboi, M., Kasuga, T. & Takano, S. 2001, *PASJ*, 53, 501
- Nyman, L. A., Johansson, L. E. B. & Booth, R. S. 1986, *A&A*, 160, 352
- Nyman, L. A., Hall, P. J. & Le Bertre, T. 1993, *A&A*, 280, 551
- Oyama, T., Miyoshi, M., Deguchi, S., Imai, H. & Shen, Z. Q. 2008, *PASJ*, 60, 11
- Ott, T., Eckart, A. & Genzel, R. 1999, *ApJ*, 523, 248

- Pardo, J. R., Alcolea, J. & Bujarrabal, V. et al. 2004, *A&A*, 424, 145
- Peeples, M. S., Stanek, K. Z. & DePoy, D. L. 2007, *Acta Astronomica*, 57, 173
- Phillips, R. B., Straughn, A. H., Doeleman, S. S. & Lonsdale, C. J. 2003, *ApJ*, 588, L105
- Reid, M. J. 1993, *ARA&A*, 31, 345
- Reid, M. J., Menten, K. M., Genzel, R. et al. 2003, *ApJ*, 587, 208
- Reid, M. J., & Brunthaler, A., 2004, *ApJ*, 616, 872
- Reid, M. J., Menten, K. M., Trippe, S. et al. 2007, *ApJ*, 659, 378
- Sjouwerman, L. O., Lindqvist, M., van Langevelde, H. J. & Diamond, P. J. 2002, *A&A*, 391, 967
- Sjouwerman, L. O., Messineo, M. & Habing, H. J. 2004, *PASJ*, 56, 45
- Tamura, M., Werner, M. W., Becklin, E. E. & Phinney, E. S. 1996, *ApJ*, 467, 645
- Wood, P. R., Habing, H. J. & McGregor, P. J. 1998, *A&A*, 336, 925

Table 1. Summary of ATCA Observations

Date	BW (MHz)	$\Delta\nu^a$ (kHz)	$\Delta v^b$ (km s <sup>-1</sup> )	$\Delta V^c$ (km s <sup>-1</sup> )	Beam ("×")	$\Delta\tau$ (min)	$\sigma^d$ (mJy)	Phase Center
86 GHz								
2006 June 9	16	62.5	0.22	−31 ~ +22	2.2 × 1.6	78	47	RA: 17:45:40.045 DEC: −29:00:27.90
2006 August 13	16	62.5	0.22	−31 ~ +22	2.3 × 1.6	135	26	as above
2007 October 21	32	250	0.87	−60 ~ +52	2.2 × 1.6	182	13	as above
2008 June 4	32	250	0.87	−60 ~ +52	5.9 × 1.2	58	48	RA: 17:45:40.038 DEC: −29:00:28.07
2008 October 3	32	250	0.87	−60 ~ +52	3.1 × 1.9	33	55	as above
43 GHz								
2008 June 3	32	250	1.74	−116 ~ +110	8.4 × 2.3	250	4	RA: 17:45:40.038 DEC: −29:00:28.07
2008 October 3	32	250	1.74	−116 ~ +110	6.3 × 3.6	29	5	as above

<sup>a</sup>: channel width in unit of kHz; <sup>b</sup>: velocity resolution corresponding to the channel width  $\Delta\nu$ ; <sup>c</sup>: velocity coverage; <sup>d</sup>: channels were binned with a width of 1 km s<sup>-1</sup> at 86 GHz and 2 km s<sup>-1</sup> at 43 GHz while mapping the SiO maser line emission, then the *rms* noise in individual channels was estimated.

Table 2. 86 and 43 GHz SiO maser sources detected in the central 4 parsecs of the GC

SN	Name	$v_{LSR}$ (km s <sup>-1</sup> )	$\Delta\Theta_x$ (")	$\Delta\Theta_y$ (")	Peak (mJy)	Intensity (mJy km s <sup>-1</sup> )	Date
86 GHz							
1	IRS 10EE	-27.7	7.74±0.10	4.23±0.40	290±20	470±80	2006 June 9
		-27.4	7.70±0.01	4.22±0.04	380±20	690±40	2006 August 13
		-27.5	7.68±0.08	4.33±0.06	340±10	700±30	2007 October 21
		-27.6	7.62±0.12	4.44±0.49	450±20	610±100	2008 June 4
		-27.5	7.67±0.71	4.26±0.50	240±4	350±110	2008 October 3
2	IRS 15NE	-11.7	0.99±0.18	11.09±0.22	139±3	392±26	2007 October 21
		-13.0	1.13±0.08	9.60±0.49	182±11	297±68	2008 June 4
43 GHz							
1	SiO-18*	-77.6	-18.88±0.03	-25.80±0.14	39.6±0.8	72.5±8.0	2008 June 3
		-78.0	-18.70±0.09	-25.16±0.07	22.9±0.3	44.7±10.0	2008 October 3
2	IRS 12N	-63.2	-3.41±0.04	-6.28±0.19	283.7±3.0	5126.0±17.9	2008 June 3
		-62.6	-3.10±0.10	-6.19±0.15	117.6±1.9	535.6±17.3	2008 October 3
3	IRS 28	-53.7	10.28±0.07	-5.43±0.39	84.6±3.0	488.6±13.9	2008 June 3
		-54.1	10.53±0.12	-5.42±0.21	129.7±1.4	458.8±17.3	2008 October 3
4	SiO-15	-35.5	-12.38±0.15	-10.40±0.40	49.9±1.0	121.8±13.9	2008 June 3
		-36.0	-12.08±0.13	-11.20±0.10	19.0±0.3	46.1±10.0	2008 October 3
5	SiO-19*	-29.4	16.09±0.11	-21.41±0.42	37.2±2.0	81.7±11.3	2008 June 3
6	IRS 10EE	-26.3	7.62±0.03	4.74±0.12	572.8±10.0	2358.0±16.0	2008 June 3
		-26.6	7.89±0.06	4.95±0.08	472.8±2.5	1982.2±20.0	2008 October 3
7	SiO-20*	-20.3	-13.94±0.03	20.91±0.57	92.4±1.0	225.2±13.9	2008 June 3
8	IRS 14NE*	-11.7	0.86±0.11	-8.01±0.51	51.0±1.0	160.8±13.9	2008 June 3
9	IRS 15NE	-13.0	0.99±0.15	11.16±0.40	46.2±1.0	269.7±16.0	2008 June 3
		-11.5	1.32±0.53	11.91±0.18	80.6±1.6	298.5±17.0	2008 October 3
10	SiO-16	+ 9.1	-26.54±0.05	-33.72±0.27	109.3±3.0	2828.0±17.9	2008 June 3
		+ 7.7	-26.33±0.22	-33.88±0.20	54.6±1.1	393.9±20.0	2008 October 3
11	SiO-21*	+ 13.8	40.74±0.08	-21.88±0.40	49.5±1.3	137.0±17.3	2008 June 3
12	SiO-22*	+ 33.6	41.28±0.06	15.63±0.22	265.8±5.0	1096.0±16.0	2008 June 3
		+ 33.4	41.12±0.26	15.80±0.23	109.0±1.2	337.7±20.0	2008 October 3
13	SiO-6	+ 52.9	35.13±0.07	31.68±0.34	111.8±6.0	2427.0±24.5	2008 June 3
		+ 52.5	35.64±0.73	31.13±0.37	56.5±1.8	295.4±22.4	2008 October 3
14	SiO-17	+ 54.1	8.00±0.05	-27.23±0.21	595.7±2.0	1887.0±20.0	2008 June 3
		+ 54.0	8.63±0.03	-27.15±0.02	112.3±0.7	281.1±10.0	2008 October 3
15	SiO-11	+ 71.5	1.66±0.05	40.70±0.15	501.3±7.0	1767.0±17.3	2008 June 3
		+ 71.1	1.93±0.12	40.66±0.07	240.1±1.6	996.8±17.3	2008 October 3
16	SiO-12	+ 80.0	-19.16±0.05	43.46±0.27	43.3±1.4	116.5±8.0	2008 June 3
		+ 80.0	-19.05±0.17	43.0790±0.12	33.0±1.2	79.1±10.0	2008 October 3
17	SiO-23*	+ 80.0	23.97±0.37	20.29±0.19	26.6±1.4	65.8±10.0	2008 October 3
18	IRS 19NW	+ 85.9	14.37±0.21	-18.28±1.14	56.6±4.5	208.4±17.3	2008 June 3
		+ 84.1	15.36±0.48	-17.23±0.21	61.6±0.5	278.1±17.3	2008 October 3

\*:new detection

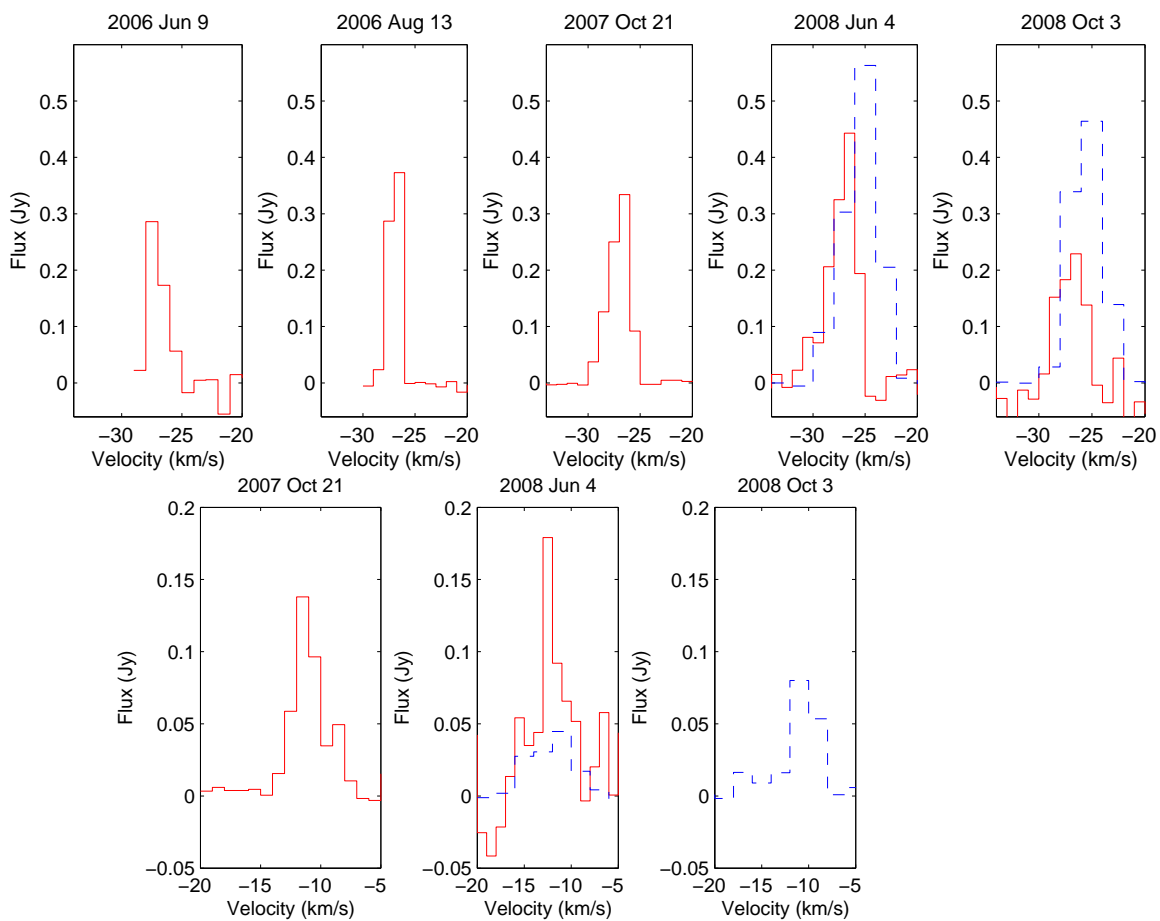


Fig. 1.— SiO maser spectra of IRS 10EE (*upper panel*) and IRS 15NE (*lower panel*) at 86 GHz (solid line) and 43 GHz (dashed line) from the ATCA observations. The velocity resolutions is  $1 \text{ km s}^{-1}$  at 86 GHz and  $2 \text{ km s}^{-1}$  at 43 GHz. The spectra were constructed at the pixel of peak brightness for SiO masers.

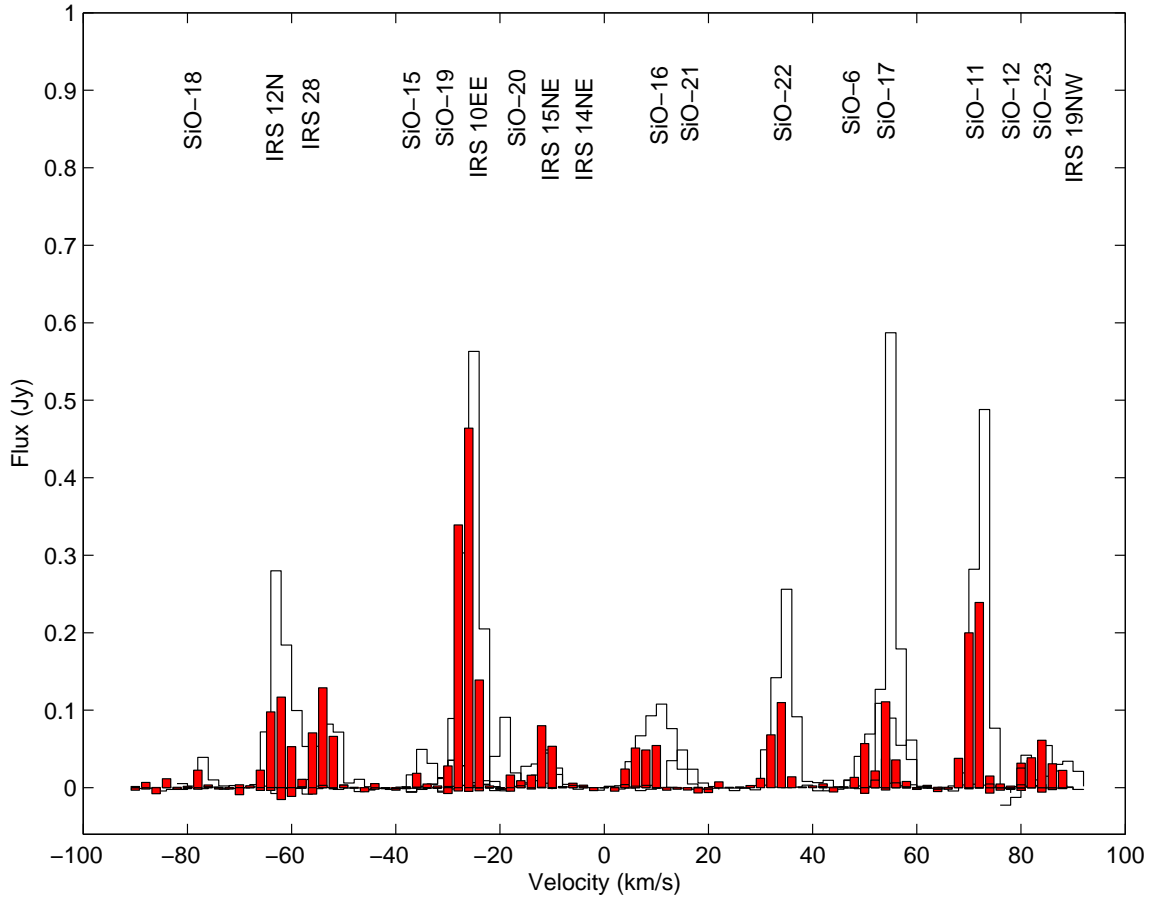


Fig. 2.— Composite spectra of 43 GHz SiO masers observed on 2008 June 3 (empty black bar) and October 3 (filled red bar).

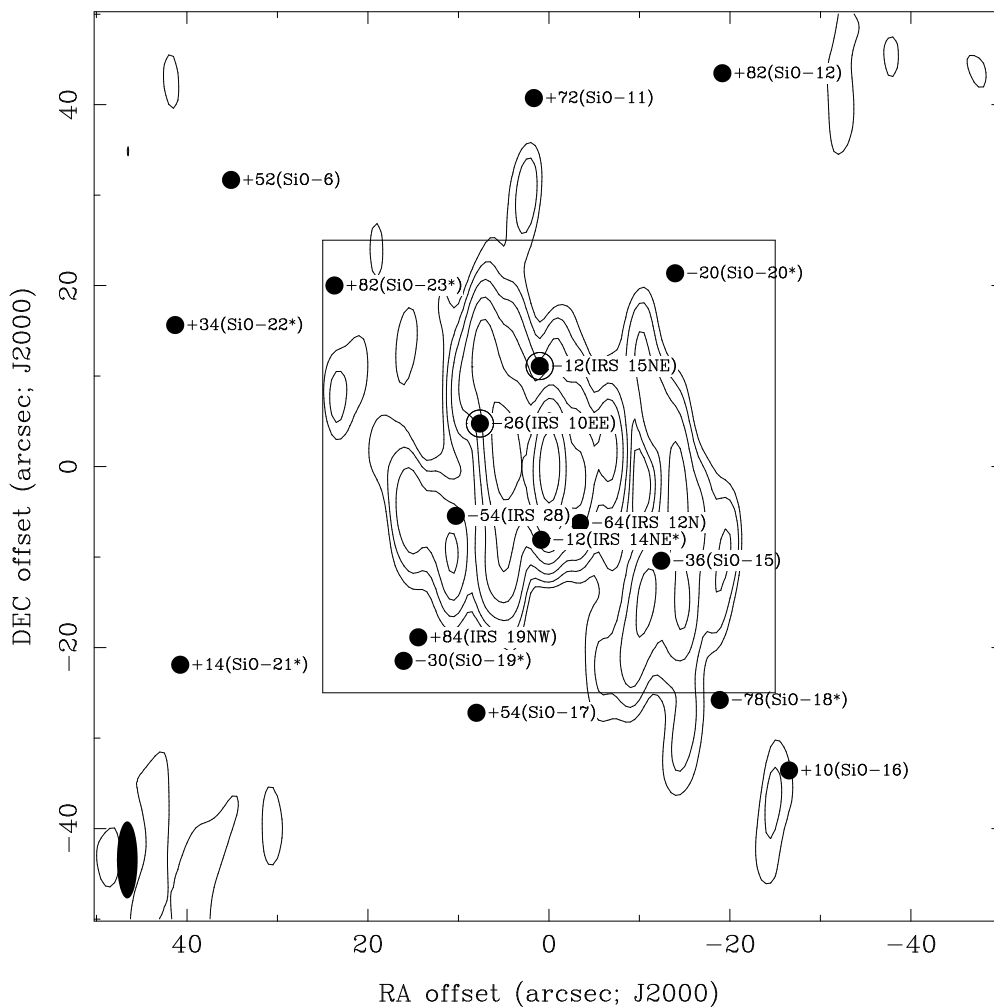


Fig. 3.— The 7 mm ATCA continuum map of the GC region observed on 2008 June 3 with a synthesized beam of  $8.''4 \times 2.''3$  (shown at the bottom left corner). The size of the region corresponds to an area of projected size 4 pc  $\times$  4 pc centered on the position of Sgr A\*. Late-type giant and supergiant stars with eighteen 43 GHz SiO maser (solid circle) emission and two 86 GHz SiO maser (open circle) emission are marked. The seven new detections are marked with \*.